

A two-phase model of galaxy formation: II. The size-mass relation of dynamically hot galaxies

Yangyao Chen,^{1,2*} Houjun Mo,^{3,4} and Huiyuan Wang^{1,2}

¹*School of Astronomy and Space Science, University of Science and Technology of China, Hefei, Anhui 230026, China*

²*Key Laboratory for Research in Galaxies and Cosmology, Department of Astronomy, University of Science and Technology of China, Hefei, Anhui 230026, China*

³*Department of Astronomy, University of Massachusetts, Amherst MA01003, USA*

⁴*Tsung-Dao Lee Institute, Shanghai Jiao Tong University, Shanghai 200240, China*

Accepted XXX. Received YYY; in original form ZZZ

ABSTRACT

In Paper-I we developed a two-phase model to connect dynamically hot galaxies (such as ellipticals and bulges) with the formation of self-gravitating gas clouds (SGCs) associated with the fast assembly of dark matter halos. Here we explore the implications of the model for the size-stellar mass relation of dynamically hot galaxies. Star-forming sub-clouds resulting from the fragmentation of the turbulent SGC inherit its spatial structure and dynamical hotness, producing a ‘homologous’ relation, $r_f \approx 100r_{\text{bulge}}$, between the size of a dynamically hot galaxy (r_{bulge}) and that of its host halo assembled in the fast regime (r_f), independent of redshift and halo mass. This relation is preserved by the ‘dry’ expansion driven by dynamical heating when a galaxy becomes gas-poor due to inefficient cooling, and is frozen due to the stop of bulge growth during the slow assembly regime of the halo. The size-stellar mass relation is thus a simple combination of the galaxy-halo homology and the non-linear stellar mass-halo mass relation. Using a set of halo assembly histories we reproduce all properties in the observed size-mass relation of dynamically hot galaxies, including the flattening in the low-mass end and the upturn in the massive end. The prediction matches observational data currently available to $z \approx 4$, and can be tested in the future at higher z . Our results indicate that the sizes of dynamically hot galaxies are produced by the dissipation and collapse of gas in halos to establish SGCs in which stars form.

Key words: galaxies: haloes – galaxies: formation – galaxies: bulges – galaxies: elliptical and lenticular, cD

1 INTRODUCTION

In the current Λ CDM cosmology, galaxies form and evolve in the gravitational potential wells of cold dark matter (CDM) halos. As gravitational systems in quasi dynamical equilibrium, galaxies are expected to obey the virial theorem at any given time, which relates the gravitational potential energy and the kinetic energy of a dynamical system. For a galaxy, the details of the relation depend on the mass distribution and velocity structure. From the perspective of galaxy formation and evolution, these are determined by the assembly of different mass components into the galaxy, energy dissipation of the star-forming gas, and the eventual support of the structure (e.g. by random motion or rotation) in the dynamical equilibrium. Clearly, the size-mass relation, which relates two of the key quantities in the virial theorem, carries important information about the formation and evolution of galaxies.

For a dynamically cold galaxy, i.e. that dominated by a stable disk, analytical investigations suggested that its size is determined by the size and spin of its host dark matter halo (e.g. Mo et al. 1998). This prediction is roughly in agreement with observational data (e.g. Mo et al. 1998; Shen et al. 2003; Somerville et al. 2018). On the other hand, the formation theory of dynamically hot galaxies, especially for elliptical galaxies, remains uncertain. Theoretical investigations

based either on empirical (Shen et al. 2003; Bezanson et al. 2009; Newman et al. 2012; Huang et al. 2017; Somerville et al. 2018), semi-analytical (Ciotti et al. 2007) or numerical (Oser et al. 2010; Hopkins et al. 2010a,b; Oser et al. 2012; McCluskey et al. 2023) approaches suggested a variety of formation scenarios for dynamically hot galaxies, such as in-situ star formation in dissipative and fast collapse of the gas component (e.g. Somerville et al. 2018), gas-rich (wet) and gas-poor (dry) mergers (e.g. Shen et al. 2003; Ciotti et al. 2007; Bezanson et al. 2009; Oser et al. 2010; Hopkins et al. 2010a,b; Oser et al. 2012; Newman et al. 2012), expansions due to significant mass loss driven by supernova (SN) and active galactic nucleus (AGN) feedback (e.g. Fan et al. 2008; Bezanson et al. 2009; Hopkins et al. 2010a), and secular evolution (e.g. Kormendy & Kennicutt 2004; Saha et al. 2010; Saha, K. et al. 2012; McCluskey et al. 2023). However, when and how these processes shape the size-mass evolution of dynamically hot galaxies are still poorly understood. There are several reasons for this. First, observational data of high- z galaxies required to constrain models directly are difficult to obtain. Second, the dissipative nature and violent collapse of the gas component in the high- z , gas-rich Universe, coupled with the expected feedback processes, are difficult to follow numerically. Third, mergers of galaxies are diverse in gas richness, mass distribution, orbital properties, and the exchange of energy and angular momentum between stars and dark matter, making their effects difficult to quantify. Finally, feedback processes are extremely difficult to model reliably, even with the state-of-the-art hy-

* E-mail: yangyaochen.astro@foxmail.com

dro simulations. The difficulty partly arises from the diverse sources of feedback whose generation, propagation, and coupling with the gas are not fully understood. For example, the EAGLE (Schaye et al. 2015) and NIHAO simulations Blank et al. (2019) both implement a purely thermal subgrid model for AGN feedback. In contrast, the TNG simulation introduces an additional kinetic-mode channel that seems crucial in quenching massive galaxies (Weinberger et al. 2017, 2018). The SIMBA simulation further incorporates an X-ray channel for AGN feedback (Davé et al. 2019) that appears to be important in producing the bimodal distribution in the stellar-to-halo mass relation of galaxies (Cui et al. 2021). Another source of the difficulty is the limitation of computational power in resolving the large dynamic range of physical scales involved in galaxy formation. For example, zoom-in simulations such as FIRE (Hopkins et al. 2018, 2023a) and SMUGGLE (Li et al. 2020) can incorporate detailed radiative feedback from stars, which is suggested to be critical in regulating small-scale gas properties. Numerical and physical convergences of stellar feedback are thus achieved only when a certain resolution threshold is reached (Deng et al. 2024).

Observationally, the size-mass relation of dynamically hot galaxies presents rich features, indicating that many processes may be relevant. Shen et al. (2003) analyzed the size-mass relation using the SDSS data at $z \approx 0.1$, and found that the relation can be well-fitted by a power law with an index of 0.56 for elliptical galaxies with stellar mass $M_* \gtrsim 10^{10} M_\odot$. A plausible formation scenario for these ellipticals was then suggested, in which the mass and size growths are both driven by repeated dry mergers with moderately bound orbits. This scenario thus indicates an energy transfer from merging galaxies to dark matter. Using a one-parameter form for the energy transfer calibrated to match the observed size-mass relation, this scenario can reproduce the observed power-law index. However, later observations (van Dokkum et al. 2008; Bezanson et al. 2009; van der Wel et al. 2014; van Dokkum et al. 2015; Newman et al. 2012; Miller et al. 2019; Mowla et al. 2019) indicated that the size-mass relation evolves significantly with redshift: at given mass, the size decreases by ≈ 0.4 dex from $z = 0$ to $z \approx 2.5$. If small ellipticals are progenitors of massive ones, the small ellipticals must obey a size-mass relation with lower amplitude, and the underlying size-mass relation must be steeper than the size-mass relation observed at a given redshift. This will lead to a strong evolution in the slope of the size-mass relation, unless the binding energy is finely tuned to depend on the redshift of the observed descendant. Meanwhile, the repeated merger scenario does not explain the flattening of the size-mass relation for lower-mass ellipticals ($M_* < 10^{10} M_\odot$) seen in Shen et al. (2003) and confirmed subsequently in other observations (e.g. Graham 2013; Lange et al. 2015; Mowla et al. 2019; Nedkova et al. 2021). In addition, for the most massive elliptical galaxies, observations also found evidence for a non-linear upturn in the size-mass relation (Bezanson et al. 2009; Lange et al. 2015; Graham 2013; Nedkova et al. 2021), which needs to be explained by theory as well.

With a proper transformation of the observed size-mass relation by relating the stellar mass with the halo mass using abundance-matching, Huang et al. (2017) found that the relation between halo virial size and galaxy size is linear for early-type galaxies, and the slope is quite independent of redshift all the way to $z \sim 3$ (see also Somerville et al. 2018). This galaxy-halo ‘homology’ is inspiring, as it suggests that the size-mass relation of dynamically hot galaxies may originate from some simple processes that relate galaxies and dark matter halos.

In our first paper of this series (Mo et al. 2023, hereafter Paper-I) we provided a framework to model the formation of dynamically hot galaxies and their supermassive black holes (SMBHs). The key to

this framework is the two-phase assembly of dark matter halos. The early, fast phase of assembly is associated with rapid cooling and collapse of gas to form a self-gravitating gas cloud (referred to as SGC). High-density gas sub-clouds formed through the fragmentation of the turbulent SGC move roughly ballistically without being significantly affected by the cloud-cloud collision and drag force from the surroundings, producing a dynamically hot system of protogalaxy. Stars that form in sub-clouds inherit the hot dynamics of the gas, producing a dynamically hot stellar system. In the late phase of slow assembly, the gas supply is reduced because of the slow accretion of new gas, ineffective cooling and feedback from SN and AGN. As demonstrated in Paper-I, without much fine-tuning, the model can reproduce a number of observations, including the correlations among SMBH mass, stellar mass of galaxies, and halo mass, as well as their evolution over the cosmic time. Relevant to this paper, the model predicts that the size of a dynamically hot galaxy is determined by the size of the SGC that forms the galaxy.

In this paper, we explore the size-mass relation of dynamically hot galaxies predicted in the framework set up in Paper-I. We will demonstrate that the physical conditions of galaxy formation expected from current cosmology naturally predicts a halo-galaxy homology. We will show that our model can not only recover all the main features seen in the observed size-mass relation at different redshift, but also can provide a clear picture regarding their physical origins. In what follows, we begin with a brief description of our model (§2). We then present our model predictions for the size-mass relation of dynamically hot galaxies and compare them with observations (§3). Finally, we summarize our main findings, compare our model with a number of other models in the literature, and discuss the potential of testing our model by future observations and simulations (§4).

2 THE MODEL

2.1 Coevolution of dark matter halos, galaxies and SMBHs

The model we developed in Paper-I is built on dark matter halo assembly histories, $M_v(z)$, defined to be the virial mass at redshift z in the main branch of a halo. Here, the virial mass is defined to be M_{200c} , the total mass enclosed in a radius, $r_v \equiv r_{200c}$, within which the mean density is 200 times the critical density of the Universe at the redshift of interest. As discussed by, e.g. Wechsler et al. (2002) and Zhao et al. (2003), the assembly of a halo can be divided into two phases: an early fast accretion phase where the halo concentration is roughly a constant, $c \approx c_f = 4$, and a late slow accretion phase where matter piles up in the outer part of the halo so that the concentration increases with time. Thus, for each assembly history, we can apply a specially tailored root-finding algorithm to obtain the transition redshift, z_f , when the specific growth rate of the halo drops below a certain fraction of the Hubble expansion rate at that redshift. Specifically, we use the solution of $\dot{V}_v/V_v = \gamma_f H(z)$ to determine z_f , where V_v is the virial velocity of the halo, $H(z)$ is the Hubble parameter, and γ_f is a constant parameter. We refer to the history at $z \geq z_f$ ($z < z_f$) as the fast (slow) assembly phase of the halo. To avoid confusion, we use a subscript ‘f’ to denote virial properties of the halo assembled in the fast phase, and use ‘v’ to denote virial properties evaluated at the redshift of interest. For example, in the fast assembly phase, we have $M_f = M_v$ and $r_f = r_v$, and in the slow assembly phase, we have $M_f < M_v$ and $r_f < r_v$.

In the fast assembly phase, the gaseous halo collapses and cools rapidly, forming a system of SGC that is turbulent and subsequently fragments into gas sub-clouds. These sub-clouds are expected to be

dense so that they move ballistically without being significantly affected by cloud-cloud collision and drag force from the surroundings. Stars formed in sub-clouds inherit their dynamics, producing a dynamically hot stellar system reminiscent of a bulge or an elliptical galaxy, and sub-clouds with low specific angular momentum can sink to the halo center to feed the SMBH. SN and AGN feedback heats and/or ejects gas from the SGC, which may suppress the star formation and SMBH growth. As discussed in §3.1 of Paper-I based on the cooling diagram, the cooling time scale, t_{cool} , of the shock-heated halo gas significantly exceeds the free-fall time scale, t_{ff} , in massive halos with $M_v \gtrsim 10^{13} h^{-1} M_\odot$, implying an inefficient gas supply to the galaxy. This, combined with the AGN feedback, regulates star formation and the growth of the SMBH, and eventually leads to the quenching of both.

Based on the above consideration, we developed a set of equations to describe the radiative cooling, star formation, SMBH growth, feedback processes, and gas evolution in individual halos to follow the evolution of different mass components, such as the stellar mass (M_*), the mass of the SMBH (M_{bh}), and the gas mass (M_g). In particular, within a given time interval in the fast assembly phase, the increases of the stellar mass and SMBH mass are assumed to be related to the increase of the halo mass by

$$\Delta M_* = \epsilon_{*,f} F_{\text{agn}} F_{\text{sn}} F_{\text{cool}} f_B \Delta M_f \quad (1)$$

and

$$\Delta M_{\text{bh}} = \alpha_{\text{cap}} \frac{M_{\text{bh}}}{M_g} F_{\text{en}} F_{\text{agn}} F_{\text{sn}} F_{\text{cool}} f_B \Delta M_f, \quad (2)$$

where f_B is the universal baryon fraction; F_{cool} determines the fraction of the accreted gas that can cool down to feed the turbulent SGC; $F_{\text{sn}} F_{\text{agn}}$ is a term to describe the fraction of cooled gas that is not affected by the SN and AGN feedback in its ability to form sub-clouds in the SGC; $\epsilon_{*,f}$ is the star formation efficiency in a sub-cloud; F_{en} is an enhancement factor describing the effects of ‘positive’ feedback in driving turbulence and producing low-angular-momentum sub-clouds to be captured by the SMBH; and $\alpha_{\text{cap}} M_{\text{bh}}/M_g$ is the fraction of sub-clouds that can be captured by the SMBH, derived by using the broad distribution of specific angular momentum in SGC.

One critical step in our model is to determine the detailed functional forms of the operators in equations (1) and (2). Based on our understanding of these processes, we adopt the following forms,

$$F_{\text{cool}}(M_f | M_{\text{cool}}, \beta_{\text{cool}}) = \frac{1}{1 + (M_f/M_{\text{cool}})^{\beta_{\text{cool}}}}; \quad (3)$$

$$F_{\text{sn}}(V_g | \alpha_{\text{sn}}, \beta_{\text{sn}}, V_w) = \frac{\alpha_{\text{sn}} + (V_g/V_w)^{\beta_{\text{sn}}}}{1 + (V_g/V_w)^{\beta_{\text{sn}}}}; \quad (4)$$

$$F_{\text{agn}}(M_{\text{bh}}, M_g, V_g | \alpha_{\text{agn}}) = 1 - \frac{\alpha_{\text{agn}} M_{\text{bh}} c^2}{M_g V_g^2}; \quad (5)$$

$$F_{\text{en}}(M_f | \alpha_{\text{en}}, \beta_{\text{en}}, M_{\text{en}}) = \frac{\alpha_{\text{en}} + (M_f/M_{\text{en}})^{\beta_{\text{en}}}}{1 + (M_f/M_{\text{en}})^{\beta_{\text{en}}}}. \quad (6)$$

For F_{cool} , the threshold $M_{\text{cool}} \approx 10^{13} h^{-1} M_\odot$ determines the regime where radiative cooling becomes ineffective, and $\beta_{\text{cool}} > 0$ characterizes the sharpness of the transition so that a larger value of β_{cool} gives a more rapid decrease of the cooling with halo mass. The supernova feedback term is assumed to depend on the maximum circular velocity of the halo, $V_g \equiv V_{\text{max}}$, and α_{sn} and V_w characterize the strength of the dependence so that the fraction of star-forming gas is reduced to α_{sn} when $V_g \ll V_w$. The quantity α_{agn} describes the AGN feedback energy injected and coupled to the SGC, and the effect is controlled by the binding energy of the SGC. The enhancement of

SMBH growth by ‘positive’ stellar feedback is expected to be significant only in low-mass halos with $M_f \lesssim M_{\text{en}}$, where stellar feedback effectively drives the turbulent motion of gas and gas cooling efficiently replenishes the cold gas, leading to turbulent motion of gas clouds within the galaxy (see, e.g. Ma et al. 2020; Hopkins et al. 2023b; Shi et al. 2023). The parameter $\alpha_{\text{en}} > 1$ represents the enhancement factor applied to the SMBH growth rate for $M_f \ll M_{\text{en}}$. The parameter M_{en} characterizes the mass scale at which positive feedback becomes unimportant, while the parameter β_{en} controls the transition rate. All these parameters have physically presumable prior ranges, but their precise values have to be calibrated by observations. As described in Paper-I, we only use the M_* - M_v relation for central galaxies (Yang et al. 2012) and the M_{bh} - $M_{*,\text{bulge}}$ relation for early-type galaxies (Graham & Sahu 2023), obtained at $z \approx 0$ to calibrate our model without further fine-tuning.

In this paper, we use a halo sample and the main-branch assembly histories generated by Monte Carlo methods based on the mass functions of Murray (2014) and the assembly history sampling method of Hearin et al. (2021), respectively. At each desired redshift, we generate a sample of 1024 halos with mass uniformly distributed in logarithmic space in the range of $10^{9.3} h^{-1} M_\odot \leq M_v \leq 10^{15.5} h^{-1} M_\odot$, and we randomly sample the main branch assembly history for each halo. Halo profile is assumed to have the NFW form (Navarro et al. 1997) with a concentration $c = c_f \approx 4$ in the fast accretion phase (e.g. Zhao et al. 2003). The characteristic radius of the profile is denoted as r_s , and the inner radius, $r_f \approx c_f r_s$, encloses the mass, M_f , that has been assembled in the fast phase. The Λ CDM cosmology adopted has $h = 0.6774$, $(\Omega_{\text{M},0}, \Omega_{\text{B},0}, \Omega_{\Lambda,0}) = (0.3089, 0.0486, 0.6911)$, and a spectral index $n = 0.9667$ and amplitude given by $\sigma_8 = 0.8159$. These are consistent with the Planck2015 results (Planck Collaboration et al. 2016). All the radii presented in this paper are physical values, rather than comoving values.

For detailed modeling of all the mass components, the list of model parameters, and the halo sampling and weighting method, please refer to the Low- z_f variant described in Paper-I. In all predictions, a log-normal scatter with $\sigma = 0.2$ dex is added to r_{bulge} (van der Wel et al. 2014), $M_{*,\text{bulge}}$ (Conroy 2013), and M_{bh} (as a rough estimate of the minimal scatter; e.g. Zhuang & Ho 2023), to mimic observational uncertainties. We note that our conclusion is robust against the choice of the adopted scatter.

2.2 The buildup of galaxy-halo homology in the wet stage

A direct prediction of our bulge formation scenario based on the formation of SGC is the galaxy-halo homology, namely a constant galaxy size-halo size ratio during the gas-rich (wet) stage of fast accretion when the cooling of halo gas is effective. If we denote the fraction of gas mass in SGC as $f_{\text{gas}} \equiv M_{\text{gas}}/M_f$, a contraction of halo gas by a factor of f_{gas} will result in self-gravitating and subsequent fragmentation of the SGC. Thus, the size of an SGC, and the characteristic size of the stellar bulge formed in it, is proportional to $f_{\text{gas}} \times r_f$. In general, we can write:

$$r_{\text{bulge}} = f_r f_{\text{gas}} r_f = f_r (1 - f_{\text{ej}}) f_B r_f. \quad (7)$$

Here, f_{ej} is the fraction of the cooled gas that is ejected from the SGC by feedback. In Paper-I, we found that, as long as cooling is effective, self-regulations by stellar and SMBH growth produce a roughly constant fraction, among the total available gas, that is affected by the feedback (see their Fig. 6). The rapid dissipation due to the high gas fraction and the rapid change of the gravitational potential in the fast assembly phase is expected to adjust the energy distribution of the gas affected by the feedback according to the gravitational potential,

regardless of the details of the feedback process. Consequently, f_{ej} , the fraction of feedback-affected gas that can escape from the SGC, is also a constant defined by the tail of the energy distribution. The value of f_{ej} can be determined by considering the boundary condition at the end of the fast assembly phase. At this moment, the gas within the galaxy is about to transit to a stable disk once the strong disturbance from rapid halo assembly stops. The stability condition, as suggested by, e.g. Mo et al. (1998, see their §3.2), implies that $f_{\text{gas}} \approx \lambda_{\text{gas}} \approx 0.04$, where λ_{gas} represents the effective spin of the gas. The value of 0.04 is similar to the median halo spin of the universal spin distribution (e.g. Bullock et al. 2001; Macciò et al. 2007; Bett et al. 2007), and is also similar to that obtained for observed galaxy disks (e.g. Shen et al. 2003; Somerville et al. 2008; Desmond & Wechsler 2015; Burkert et al. 2016; Somerville et al. 2018). Given that the universal baryon fraction $f_B = 0.16$, approximately 3/4 of the gas is expected to be ejected to reduce f_{gas} to the stable value. Thus, we set $f_{\text{ej}} = 3/4$ as the fiducial value in our model. Finally, f_r is a constant factor specific to the definition of the bulge size. As found previously (e.g. Miller et al. 2019; Mowla et al. 2019; Suess et al. 2019; van der Wel et al. 2024), adopting different definitions of radius can result in different size-mass relations. The factor $f_r \leq 1$, with its value calibrated by observational data, is included to take account of the arbitrariness in the definition. We use the observational results obtained by Shen et al. (2003) for present-day elliptical galaxies with stellar mass $M_* \approx 5 \times 10^{10} h^{-1} M_\odot$ to calibrate f_r , and we obtain $f_r = 0.26$. Their choice of radius is the r -band half-light radius, which is commonly adopted in the literature. Taking all the factors as described above, equation (7) approximately gives

$$r_{\text{bulge}} \approx 0.01 r_f, \quad (8)$$

or

$$r_f \approx 100 r_{\text{bulge}}, \quad (9)$$

regardless of the halo mass and redshift, as long as the halo is in the fast assembly phase and radiative cooling is effective. We note that the definition of r_{bulge} is not unique in observations and may have systematic differences depending on factors such as sample selection, the method used to fit the light profiles and to handle the wavelength dependence. As shown by van der Wel et al. (2024), for quiescent galaxies, the 2-D half-stellar-mass radius is approximately 0.1–0.14 dex smaller than the optical half-light radius for galaxies with $M_* > 10^{10} M_\odot$ at $z < 2.5$ (see their §2.4), while the 3-D (deprojected) half-stellar-mass radius is about 0.05 dex larger than the 2-D half-stellar-mass radius (see their §2.6). Consequently, the systematic difference between the 3-D half-stellar-mass radius and the 2-D optical half-light radius is largely canceled out, leaving these two radii consistent with each other within 0.1 dex. Hence, r_{bulge} modeled and calibrated here can serve as a proxy for both the 2-D half-light radius in the optical band and the 3-D half-stellar-mass radius.

2.3 The preservation of the galaxy-halo homology in the dry stage

For massive halos that exceed the cooling threshold (M_{cool}) in their fast assembly phase, the gas supply is cut off and the galaxy becomes a gas-poor (dry) system that enters into the regime of quenching. However, since halo is still in the fast assembly regime, the gravitational potential of the halo is still changing rapidly.

One process that may be responsible for the late growth of giant ellipticals is gas-poor minor merger (Naab et al. 2009; Bezanson et al. 2009; Hopkins et al. 2010a). As small galaxies are in general

less bound by self-gravity than massive ones, minor mergers inject positive binding energy into the merger remnant, which makes the remnant expand without changing the total stellar mass significantly. However, even with relatively strong energy injection, minor mergers alone may not be able to explain the rapid size growth of giant ellipticals (Hopkins et al. 2010b). Recent hydrodynamic simulations show that there may be more channels for the energy injection, especially during the fast phase of halo assembly. These channels, collectively referred to as ‘dynamical heating’, include all processes that can repeatedly scatter stars. The sources of scattering can be very diverse. Giant molecular clouds, spiral arms, global asymmetries, feedback-driven outflows, cosmic accretion, mergers, and close interaction with satellites can all have their impacts (see, e.g. McCluskey et al. 2023, for a summary).

Despite the details, the effects of dynamical heating in a fast accreting halo may be simple to describe. The halo profile in the fast assembly phase is found to be almost universal, an NFW profile with a nearly constant concentration parameter $c \approx c_f$ (Zhao et al. 2003; Lu et al. 2006). Only the size and amplitude of the halo density profile change with time. This is a homology in the halo population. Thus, the dynamical heating due to frequent and repeated scattering in the fast regime has a global effect that causes the expansion of the halo as a whole without changing its self-similar structure (homology). Consequently, all the collisionless components, including the central galaxy and the inner region ($r < r_s$) of the halo, experience similar evolution. The bulge size-halo size ratio, therefore, remains unchanged during the evolution in this regime. Such a growth thus preserves the galaxy-halo homology that has built up in the wet stage.

Putting the above modeling together, we obtain a prediction for the bulge size-halo size relation for dynamically hot galaxies, which is $r_f \approx 100 r_{\text{bulge}}$ throughout the fast assembly phase. The physical origin of this relation is clear and simple:

- (i) the homology is built up from *wet contraction* to form self-gravitating gas clouds that are turbulent and fragment rapidly to form dense star-forming sub-clouds, and
- (ii) for massive halos that can enter the gas-poor stage, the homology is preserved by *dry expansion* driven by dynamical heating.

3 INTERPRETATION OF THE OBSERVED SIZE-MASS RELATION FOR DYNAMICALLY HOT GALAXIES

3.1 Model predictions and comparisons with observational data

The gray dots in Fig. 1 show our model prediction for the size and mass of individual dynamically hot central galaxies. Here, we define dynamically hot galaxies as those with the bulge mass fraction $f_{\text{bulge}} = M_{*,\text{bulge}}/M_* > 0.75$, and we have tested that the results are robust against the choice of the threshold. Results at four different redshifts, from $z = 0.1$ to $z = 3.25$, are shown in the four panels, respectively. Each dot is color-coded according to its sampling weight, w_{samp} , defined to be the number of occurrences of such a galaxy in a cubic box with a side length $l_{\text{box}} = (75 h^{-1} \text{Mpc})^3 \approx (100 \text{Mpc})^3$. The black line is a linear (in log-log space) fitting for all galaxies with $M_{*,\text{bulge}} \geq 10^{10} h^{-1} M_\odot$, and represents a power-law with an index ≈ 0.6 and an amplitude that decreases systematically with increasing redshift. For comparison, red squares with error bars in the first panel are the size-mass relation obtained by Shen et al. (2003) for local elliptical galaxies using the SDSS data. The red line shows a linear fit to high-mass galaxies ($M_* \gtrsim 10^{10} h^{-1} M_\odot$), with the shaded area indicating the residual of the fitting. The power-law index of this

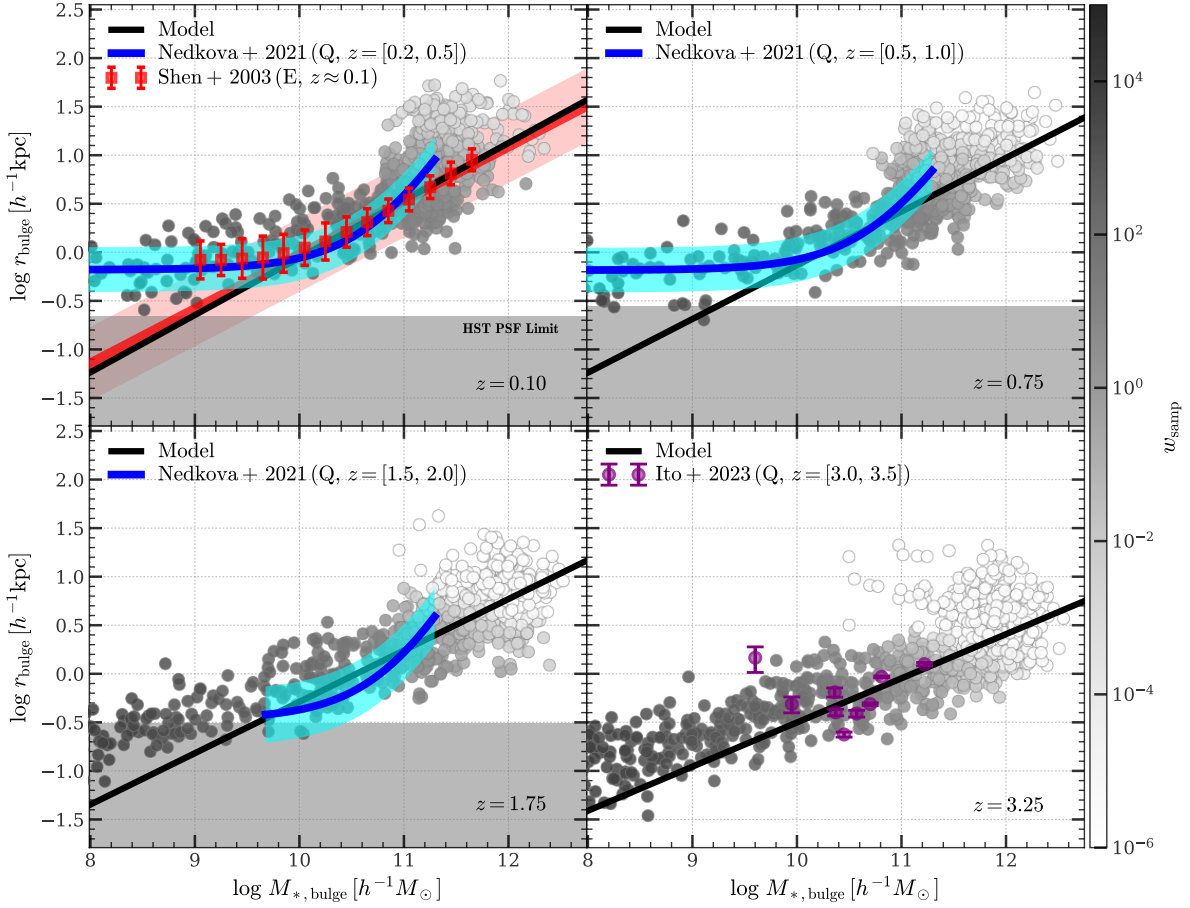


Figure 1. Size-mass relation of dynamically hot galaxies. Results at $z = 0.1, 0.75, 1.75$ and 3.25 are shown in **four panels**, respectively. Galaxies with bulge mass fraction $f_{\text{bulge}} > 0.75$ are included. In each panel, **gray scatter points** are our model prediction for the bulge size r_{bulge} and bulge stellar mass $M_{*,\text{bulge}}$ of individual galaxies, color-coded by the sampling weight (w_{samp}) according to the colorbar. **Black solid line** is a linear fit for galaxies with $M_{*,\text{bulge}} > 10^{10} h^{-1} M_{\odot}$. In the first panel, **red squares** with error bars are size-mass relation obtained by Shen et al. (2003, see their Fig. 8) for SDSS early-type (E) galaxies defined by $^{0.1}(g-r) > 0.7$ at $z \approx 0.1$, where r -band Sérsic half-light radius is used as galaxy size. Here, a constant mass-to-light ratio is used to convert their r -band Sérsic absolute magnitude to stellar mass. **Red line** is their linear fit for high-mass galaxies (see their Table 1), which has a logarithmic slope of 0.56. In each of the first three panels, **blue curve** is the size-mass relation obtained by Nedkova et al. (2021, see their Fig.10 and Table 2) using HST images for quenched (Q) galaxies defined by a UVJ color-color cut at the redshift range indicated in the legend. The 5000 Å half-light radius is used as their galaxy sizes. Gray shaded area in the bottom of the panel indicates the size below $\text{FWHM}_{\text{F160W}}/2$ of the point spread function. The red and blue shading areas indicate their residuals of fitting. In the last panel, **purple dots** with errorbars show the measurements obtained by Ito et al. (2023) using images from a number of recent JWST surveys for quenched galaxies selected by multiple color-based criteria at $3 \leq z \leq 3.5$. Here the 5000 Å effective radius along the semi-major axis is used as their galaxy size. Only the ‘good-fit’ galaxies are included (see their Table 2). This figure indicates that our model can reproduce the observed size-mass relations, including the slope of high-mass galaxies, the non-linearity, and the evolution over the cosmic time (see §3.1 for the details).

relation is 0.56. Their result for high-mass galaxies has nearly the same amplitude as our results, as is expected from the fact that it is used to calibrate the only free parameter f_t in our model. However, our prediction for the slope is also consistent with the data, indicating that our model can match the observed mass dependence of galaxy size. In the same figure, we also show the results for quenched galaxies obtained by Nedkova et al. (2021) from HST images, and by Ito et al. (2023) from JWST images. At $M_{*,\text{bulge}} \approx 10^{10}-10^{11} h^{-1} M_{\odot}$, the model predictions match the observational results well, indicating that our model can reproduce the observed redshift evolution of the size-mass relation.

An interesting feature of the model prediction is the non-linearity at both the low- and high-mass ends. At $M_{*,\text{bulge}} \leq 10^{10} h^{-1} M_{\odot}$, the predicted relation is flattened, with an asymptotic power index smaller than $1/3$ (see below). This flattening was first seen in Shen et al. (2003) at $z \approx 0.1$, as shown by the red symbols in the first

panel of our figure, and confirmed by subsequent observations at different redshifts (e.g. Graham 2013; Lange et al. 2015; Mowla et al. 2019; Miller et al. 2019; Nedkova et al. 2021). At the high-mass end, $M_{*,\text{bulge}} > 10^{11} h^{-1} M_{\odot}$, the predicted relation shows an upturn, which is dominated by massive and rare objects. This upturn is seen in all bands analyzed by Lange et al. (2015), and seen at all redshifts below $z = 2$ in Nedkova et al. (2021). To deal with the non-linearity, these authors adopted a double-power-law model to fit the observed size-mass relation over the full stellar mass range covered by the data. The results of Nedkova et al. (2021) are shown in Fig. 1 for comparison, with blue curves depicting the fitting functions and shaded areas representing the root-mean-square of the residual. Our results reproduce the non-linearity in both ends, and match the observations at all redshifts. The presence of the non-linearity makes the linear fitting uncertain against the choice of the lower bound of the stellar mass, the choice of the likelihood function, and the galaxy

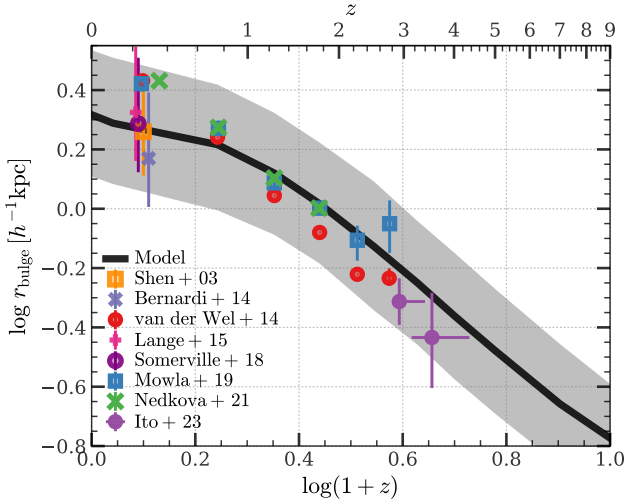


Figure 2. Size evolution of dynamically hot galaxies at $M_{*,\text{bulge}} = 5 \times 10^{10} M_{\odot}$ up to redshift $z = 9$. **Black line** shows the median size at each given redshift predicted by our model, with the gray shading area indicating the $1-\sigma$ (16%-84%) quantiles. **Colored markers** are results at $z \lesssim 4$ obtained by different observations (Shen et al. 2003; Bernardi et al. 2012; van der Wel et al. 2014; Lange et al. 2015; Somerville et al. 2018; Mowla et al. 2019; Nedkova et al. 2021; Ito et al. 2023). See §3.1 for a detailed description of this figure.

sample used. In the following, we quantify the size-mass relations using two alternative methods that are more robust against these issues.

The first method is to only consider the evolution of the galaxy size in a narrow bin around a fixed mass. Fig. 2 shows the evolution of the size-mass relation at a fixed mass of $M_{*,\text{bulge}} = 5 \times 10^{10} h^{-1} M_{\odot}$. For comparison, we also show the size evolution obtained from various observations covering a range of redshift from $z \sim 0$ to $z \approx 3.5$. Results obtained from different data and analyses are consistent with each other, with a variance of ≈ 0.2 dex. Our model prediction follows closely the observational trend, showing a decrease of ≈ 0.5 dex in galaxy size from $z = 0$ to $z = 3.5$.

The second method is to fit the size-mass relation with a non-linear function. As discussed around equation (7), the size of the bulge is a constant fraction of the halo radius r_f in the fast assembly phase. Given the relation between the mass and radius of dark matter halos, the size-mass relation can be understood in terms of the halo mass-stellar mass relation that is established in the fast assembly phase. In terms of causality, the bulge size should be considered as the independent variable, while the bulge mass should be considered as a function of the bulge size. Thus, using the double-power-law form of the stellar mass-halo mass relation found by Yang et al. (2012), we can fit the size-mass relation at a given redshift by a double-power-law function of the form

$$M_{*,\text{bulge}} = M_{0,\text{bulge}} \frac{(r_{\text{bulge}}/r_{0,\text{bulge}})^{\alpha_{\text{bulge}}+\beta_{\text{bulge}}}}{(1+r_{\text{bulge}}/r_{0,\text{bulge}})^{\beta_{\text{bulge}}}}. \quad (10)$$

The best-fit parameters, $M_{0,\text{bulge}}$, $r_{0,\text{bulge}}$, α_{bulge} , and β_{bulge} , are listed in Table 1, and we show the fitting functions at $z \leq 9$ in the center panel of Fig. 3. For comparison, we show the r_f - M_f relation of halos, which has a power-law index of $\beta_f = 1/3$ at any redshift. We also show the r_f - M_f relation obtained from a sample of simulated halos at $z = 0$ (sample $S_{h,\text{large}}$ defined in Paper-I). This relation has a power-law index $\beta_{f,\text{max}} = 0.41$, which is larger than β_f due to the fact that halos with higher mass have lower concentrations,

or equivalently, later transitions from the fast assembly phase to the slow assembly (see §3.3 of Paper-I). The size-mass relations obtained from different redshifts are roughly parallel to each other in the log-log space. At $M_{*,\text{bulge}} \sim 10^{10.5} h^{-1} M_{\odot}$, the predicted size-mass relation is roughly parallel to the r_f - M_f relation, with a slope close to $\beta_{f,\text{max}}$. At $M_{*,\text{bulge}} < 10^{9.5} h^{-1} M_{\odot}$, the size-mass relation is flattened, with a slope even less than β_f . At the massive end, $M_{*,\text{bulge}} > 10^{11} h^{-1} M_{\odot}$, the size-mass relation shows an upturn, produced by the size growth during the period where the mass growth is stalled. The predicted increase is about 1 dex (0.5 dex) from $z = 9$ ($z = 3$) to $z = 0$.

Since the growth of the bulge in a fast accreting halo is associated with the growth of its SMBH, bulge properties are expected to be tightly correlated with the SMBH mass, M_{bh} . The size of a dynamically hot galaxy, r_{bulge} , is thus expected to be correlated with M_{bh} . To see this, we fit the r_{bulge} - M_{bh} relations predicted by our model at different redshifts for dynamically hot galaxies using the same functional form as equation (10). The best-fit parameters are listed in Table 1 with a subscript ‘bh’, and the fitting functions are plotted in the right panel of Fig. 3. The r_{bulge} - M_{bh} relation shows similar behavior to the r_{bulge} - $M_{*,\text{bulge}}$ relation at low redshift. This is expected because of the M_{bh} - $M_{*,\text{bulge}}$ relation observed (Greene et al. 2020; Graham & Sahu 2023; Zhuang & Ho 2023, e.g.) at $z \approx 0$ and reproduced by our model (see Fig. 7 of Paper-I). The observed M_{bh} - $M_{*,\text{bulge}}$ relation has a power-law index about $3/2$ for early-type galaxies with $M_{*,\text{bulge}} \gtrsim 10^{10} h^{-1} M_{\odot}$. This, combined with the power-law indices β_f and $\beta_{f,\text{max}}$, gives the solid and dashed black lines in the right panel of Fig. 3, respectively. Our predicted r_{bulge} - M_{bh} relation for $M_{\text{bh}} \gtrsim 10^7 h^{-1} M_{\odot}$ at $z \approx 0$ has the expected power-law behavior. At higher redshift, M_{bh} is shifted leftward relative to $M_{*,\text{bulge}}$, because low-mass SMBHs have not reached the self-regulation regime and do not follow the M_{bh} - $M_{*,\text{bulge}}$ scaling relation.

For reference, we also show the bulge size-halo mass (M_f) relations for dynamically hot galaxies at different redshifts in the left panel of Fig. 3. These relations are obtained by fitting the model predictions at individual redshifts with a power-law function of the form

$$\log r_{\text{bulge}} = \left(\frac{M_f}{M_{0,f}} \right)^{\beta_f}, \quad (11)$$

and the best-fit parameters are also listed in Table 1. At all redshifts, the power-law index β_f is contained in a narrow range from 0.33 to 0.37. At a given M_f , the bulge size increases as redshift decreases due to the decrease of the density threshold, approximately 200 times the mean density of the Universe, required for the collapse of CDM halos. In the following, we use these results to interpret the physical origin of the size-mass relation of dynamically hot galaxies.

3.2 The physical origin of the size-mass relation

Given that the observed features in the size-mass relation are well reproduced by our model, we can use our model to understand the physical origin of these features. The basic underpinning is a simple combination of the homology relation, $r_f \approx 100 r_{\text{bulge}}$, and the stellar mass-halo mass relation (SMHMR), at any given redshift z , as described below.

- (i) At $M_{*,\text{bulge}} \approx 10^{10.5} h^{-1} M_{\odot}$ ($M_f \approx 10^{12} h^{-1} M_{\odot}$), the star formation efficiency (described by $M_{*,\text{bulge}}/M_f$) reaches its peak, which signals the regime where AGN feedback is about to become effective. Consequently, the growth of the stellar mass follows the growth

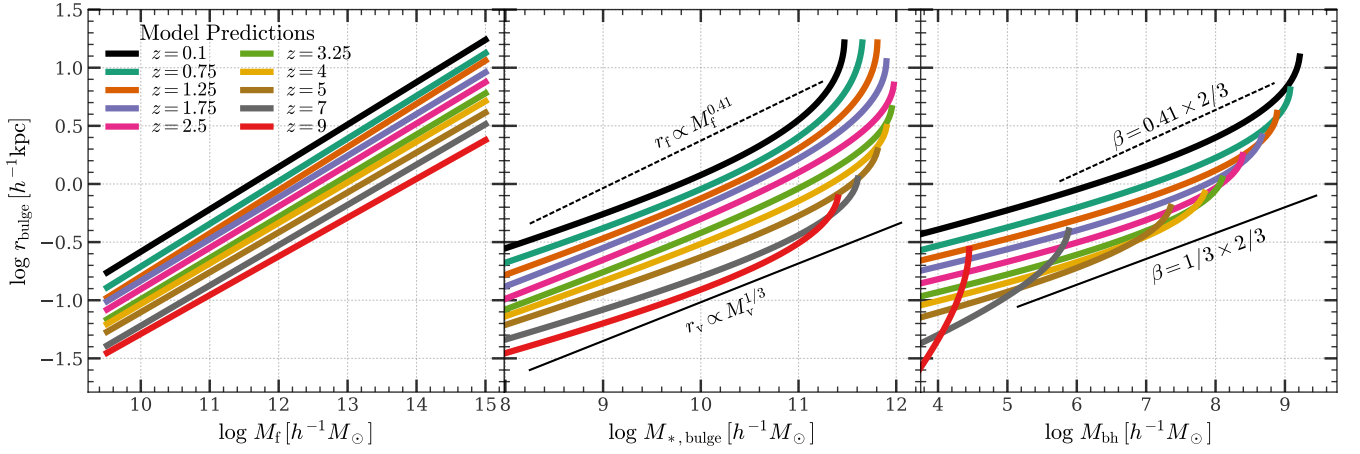


Figure 3. Size-mass relation of dynamically hot galaxies predicted by our model up to $z = 9$. The **left panel** shows the bulge size (r_{bulge})-halo mass (M_f) relations. Curves with **different colors** show the fitted relation at different redshifts, as labeled in the legend. The **center panel** shows the bulge size (r_{bulge})-bulge mass ($M_{*,\text{bulge}}$) relations (referred to as size-mass relations). The **black dashed line** indicates the r_f - M_f relation (arbitrarily scaled) of halos fitted from simulated halo at $z = 0$, with a power-law index $\beta_{f,\text{max}} = 0.41$. The **black solid line** indicates the r_v - M_v relation (arbitrarily scaled) at arbitrary redshift, which by definition has a power-law index of $\beta_v = 1/3$. The **right panel** is similar but shows the bulge size-SMBH mass (M_{bh}) relations. Black dashed and solid lines are obtained by scaling the power-law indices β_v and $\beta_{f,\text{max}}$ with $2/3$ to account for the M_{bh} - $M_{*,\text{bulge}}$ scaling relation for high-mass systems ($M_{*,\text{bulge}} \gtrsim 10^{10} h^{-1} M_\odot$). See §3.1 for a detailed description of this figure and §3.2 for a physical interpretation. For the list of fitted parameters, see Table 1.

Table 1. Best-fit parameters of the bulge size (r_{bulge})-halo mass (M_f) relation, bulge size-bulge mass ($M_{*,\text{bulge}}$) relation, and bulge size-SMBH mass (M_{bh}) relation of dynamically hot galaxies predicted by our model at different redshift (z). See Fig. 3 for a plot of fitted functions and §3.1 for a detailed description. No observational data for r_{bulge} are currently available at $z \gtrsim 4$. The root-mean-square error, $\sigma_{\log r_{\text{bulge}}}$, is listed in reference.

z	$\log M_{0,f}$ [$h^{-1} M_\odot$]	β_f	$\sigma_{\log r_{\text{bulge}}}$ [dex]	$\log r_{0,\text{bulge}}$ [$h^{-1} \text{kpc}$]	$\log M_{0,\text{bulge}}$ [$h^{-1} M_\odot$]	α_{bulge}	β_{bulge}	$\sigma_{\log r_{\text{bulge}}}$ [dex]	$\log r_{0,\text{bh}}$ [$h^{-1} \text{kpc}$]	$\log M_{0,\text{bh}}$ [$h^{-1} M_\odot$]	α_{bh}	β_{bh}	$\sigma_{\log r_{\text{bulge}}}$ [dex]
0.1	11.6	0.364	0.226	0.515	12.34	-0.716	4.62	0.331	0.565	11.2	-1.86	8.96	0.31
0.75	11.93	0.367	0.227	0.425	12.33	-0.496	4.29	0.333	0.455	11.87	-3.11	10.6	0.4
1.25	12.14	0.371	0.23	0.515	12.59	-0.652	4.12	0.326	0.334	12.24	-4.05	12.1	0.479
1.75	12.32	0.359	0.219	0.696	13.09	-1.33	4.53	0.304	0.224	12.39	-4.73	13	0.523
2.5	12.54	0.356	0.208	0.867	13.8	-2.96	6.07	0.297	0.153	12.74	-6.32	14.7	0.567
3.25	12.8	0.354	0.205	0.807	14.19	-4.24	7.5	0.326	0.0528	12.84	-7.44	15.7	0.566
4	12.96	0.349	0.201	0.656	14.32	-4.64	8.13	0.362	0.00251	12.85	-8.5	16.6	0.556
5	13.21	0.343	0.208	0.425	14.33	-4.61	8.43	0.411	-0.0477	12.21	-9.06	16.3	0.537
7	13.52	0.347	0.2	0.0226	14.06	-3.81	8.15	0.476	-0.249	8.629	-5.09	9.18	0.492
9	13.87	0.333	0.209	-0.299	13.43	-2.58	7.1	0.488	-0.5	5.258	-1.37	2.68	0.56

of the halo mass (i.e. $d \log M_{*,\text{bulge}} / d \log M_f = 1$), and the growth of the bulge size follows the growth of the halo size due to the wet contraction. The size-mass relation thus has a power-law index close to β_f , the power index of the size-mass relation for halos in fast assembly. Note that dynamically hot galaxies ($f_{\text{bulge}} > 0.75$) have halo transition redshift, z_f , close to the redshift z in question, and hence $M_f \approx M_v$, $M_{*,\text{bulge}} \approx M_*$. The shape of the $M_{*,\text{bulge}}$ - M_f relation of these galaxies (see Appendix A) thus follows that of their M_* - M_v relation (e.g. Yang et al. 2003, 2012; Behroozi et al. 2013).

- (ii) At $M_{*,\text{bulge}} < 10^{9.5} h^{-1} M_\odot$, the star formation efficiency is suppressed by SN feedback, which produces a lower $M_{*,\text{bulge}}$ for a given M_f than expected from the peak of the star formation efficiency. However, the size of the bulge is still controlled by the wet contraction, and thus by r_f according to the homology relation. This produces a flattening in the size-mass relation, where the power-law index is smaller than β_f , or even smaller than β_v , depending on the star formation efficiency.
- (iii) At $M_{*,\text{bulge}} > 10^{10.5} h^{-1} M_\odot$, the star formation efficiency can be reduced significantly by AGN feedback, again leading to a lower $M_{*,\text{bulge}}$ at given M_f than that expected from the star formation at the peak. The galaxy-halo homology is again fixed by the wet

contraction, which produces a steepening in the size-mass relation with a power index larger than β_f .

- (iv) In the massive end, $M_{*,\text{bulge}} > 10^{11} h^{-1} M_\odot$, or $M_f > 10^{13} h^{-1} M_\odot$, star formation is quenched due to ineffective cooling, producing a dry system with fixed stellar mass. However, the homologous galaxy-halo size relation is still preserved by dynamical heating driven by the fast halo assembly. The synergy of the fixed stellar mass and the expansion of the bulge results in a significant upturn in the high-mass end of the size-mass relation.
- (v) At a given bulge mass, the increase of the bulge size with decreasing redshift is produced by the increase of r_f due to the decrease of the density threshold required for the collapse of CDM halos.

The above interpretations, including the physical origin of the galaxy-halo homology, the non-linear transformation due to the incorporation of the SMHMR, and the time evolution due to the Hubble expansion, are summarized schematically in Fig. 4. This figure also includes the formation scenario of disk galaxies presented in Mo et al. (1998). A mixed system of bulge and disk may then be considered as a combination of the two components, with the mass ratio between the two determined by the transition time of the halo. The effective radius of such a system is expected to fall between that of the dynamically hot galaxy (classical bulge) and dynamically cold

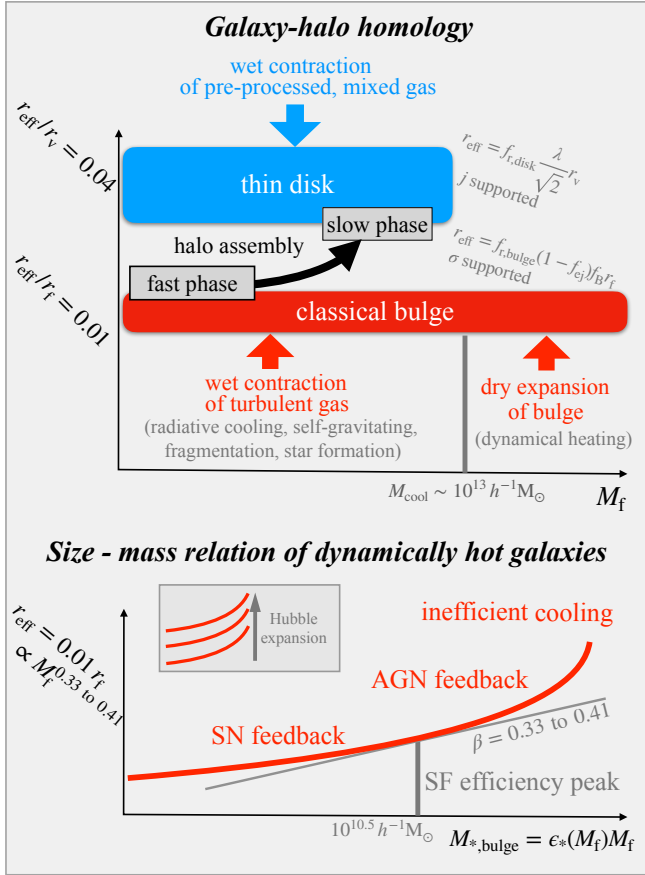


Figure 4. A schematic figure showing the physical origin of galaxy-halo homology (top panel, see §2 for the details) and the size-mass relation of dynamically hot galaxies (bottom panel, see §3 for the details). In both panels, we show the properties in both axes in a logarithmic scale. This figure demonstrates that the galaxy-halo homology (i.e. constant ratio between the galaxy size and halo size) of dynamically hot component is built up by the *wet contraction* of turbulent gas, and preserved by the *dry expansion* of the stellar bulge. Consequently, the size-mass relation of dynamically hot galaxies at a given redshift directly reflects the stellar mass-halo mass relation, which is shaped by *cooling and feedback processes*, and the evolution of the size-mass relation originates from the evolution of the halo size-halo mass relation.

galaxy (thin disk), i.e. between $0.01 r_f$ and $0.04 r_v$, which is consistent with the scaling relations found in observations with abundance matching (Kravtsov 2013; Huang et al. 2017; Somerville et al. 2018) and gravitational weak lensing (Mishra et al. 2023).

4 SUMMARY AND DISCUSSION

We use the two-phase model developed in Paper-I to predict the size-mass relation for dynamically hot galaxies (such as ellipticals and bulges). We find a remarkable agreement between our model predictions and the observed size-mass relation up to $z \approx 4$, with all observed features well reproduced. We provide a clear and physically-motivated interpretation regarding the origin of the size-mass relation. Our analyses and results are summarized as follows.

- (i) *Two-phase assembly of halos:* Our model is based on the fact that the growth of cold dark matter halos consists of an early fast phase of assembly followed by a slow assembly phase.

- (ii) *Build-up of the galaxy-halo homology:* In the fast assembly phase, rapid radiative cooling causes rapid collapse of the halo gas, producing a turbulent gas cloud. The contraction of the gas is halted once the cloud becomes self-gravitation and fragments to form dense sub-clouds that can move ballistically. Stars that form in sub-clouds inherit their spatial distribution and dynamical hotness, producing a stellar bulge with a characteristic size (r_{bulge}) proportional to the halo virial radius (r_f). Detailed modeling and calibration give a homologous relation, $r_f \approx 100 r_{\text{bulge}}$, independent of the halo mass and redshift.
- (iii) *Preservation of the galaxy-halo homology:* For a massive halo with mass exceeding the cooling threshold in the fast phase, the gas supply is cut off and the stellar bulge becomes a dry system in the regime of quenching. The dry expansion caused by dynamical ‘heating’ associated with the fast halo assembly preserves the galaxy-halo homology, extending the halo size-bulge size relation to the end of the fast assembly phase.
- (iv) *Freeze of the bulge growth:* As a halo enters the slow assembly phase, the reduced gas fraction and the longer time for cooling provide the condition for the formation of a dynamically cold disk, thereby terminating the mass growth of the bulge. The stable gravitational potential also reduces dynamical heating, which freezes the growth of the bulge size. The bulge mass and size are then preserved during the entire phase of the slow assembly.
- (v) *The size-mass relation of dynamically hot galaxies:* The combination of the galaxy-halo homology relation and the stellar mass-halo mass relation is the key to producing the size-mass relation. The non-linearity in the size-mass relation is a direct consequence of the star formation efficiency ($M_{*,\text{bulge}}/M_f$) in halos, which is controlled by gas cooling and feedback, and the time evolution of the size-mass relation is a direct reflection of the halo radius at a given halo mass, which increases with time due to Hubble expansion.
- (vi) *Comparison with observations:* A comparison of our model prediction with observations at $z \lesssim 4$ indicates that the model is able to reproduce the observed size-mass relation, including its slope at $M_{*,\text{bulge}} > 10^{10} h^{-1} M_{\odot}$, the non-linear flattening in the low-mass end, the non-linear upturn in the high-mass end, and the time evolution of the relation (Figs. 1 and 2).
- (vii) *Prediction for future observations:* Our model makes predictions for the size (r_{bulge})-halo mass (M_f) relation, size-bulge mass ($M_{*,\text{bulge}}$) relation, and size-SMBH mass (M_{bh}) relation, of dynamically hot galaxies at $z \gtrsim 4$ (Fig. 3), which can be tested by future observations.

The galaxy-halo homology relation of dynamically hot galaxies, $r_f \approx 100 r_{\text{bulge}}$, can be tested using weak gravitational lensing observations. Investigations in this direction have been conducted (e.g. Mishra et al. 2023), and a nearly constant $r_{\text{bulge}}-r_v$ ratio has been identified, albeit with some subtle dependence on the stellar mass. Our analysis suggests that the correlation should be tested on central elliptical galaxies, and the halo property to be inferred should be $r_f \approx 4 r_s$, where r_s is the characteristic radius of the NFW profile. The predicted constant $r_{\text{bulge}}-r_f$ ratio, with little secondary dependence on other properties, such as stellar mass, halo mass and redshift, can then be checked by observations.

Our model for the formation of dynamically hot central galaxies suggests that the galaxy-halo connection may be more properly described by M_* and M_f , rather than by M_* and M_v , as the use of M_f provides a more precise prediction of M_* and avoids the uncertainties in the definition of halo boundary. The homology relation of dynamically hot galaxies also suggests that the bulge size may also contain information about the halo mass. Thus, the synergistic use of galaxy size and stellar mass may provide a more accurate estimate of the halo mass, which can be calibrated and applied to observations. The

predicted tight relation between the bulge size and the SMBH mass suggests that this relation should be analyzed to provide additional constraints on SMBH mass in observations.

Our model includes only central galaxies, thus missing environmental effects specific for satellite galaxies. However, as the bulge is not as extended as the disk, tidal stripping is expected to have only minor effects on the structure of the bulge. Observations by Guo et al. (2009) from the SDSS support this expectation. Our model does not explicitly incorporate mergers in the growth of the bulge. Mergers are expected to be important for the formation of massive ellipticals. The effect of minor mergers on the mass growth is expected to be as small as $\approx 10\%$, as indicated by numerical simulations (e.g. Hopkins et al. 2010b) and semi-analytic models (e.g. Lotz et al. 2011). Furthermore, their effects on the size growth have already been included in the dry expansion. For major mergers, particularly those involving gas-rich progenitors, there are debates as to whether the in-situ star formation in the merger remnant or the accretion of ex-situ stars dominates the bulge growth. The in-situ mass and size growths have been included in our model for the star formation in the SGC. The ex-situ accretion from major mergers yields approximately a 1:1 mass-size growth, thus is degenerate with the in-situ growth. Consequently, the inclusion of mergers is not expected to change the main conclusion of our model for the size-mass relation of dynamically hot galaxies. Numerical simulations have been used to disentangle the in-situ versus ex-situ contributions (e.g. Oser et al. 2010). However, current simulations are yet to predict sizes for elliptical galaxies to match observational data (Mishra et al. 2023), and need improvements before reaching any definitive conclusions. Future observations of galaxies in the high- z Universe, where ex-situ accretion may play a less important role, may help to resolve the degeneracy (e.g. Ji & Giallisco 2022, 2023). In addition, detailed analyses of the profiles of local galaxies using spatially resolved spectroscopy and stellar population synthesis can also shed light on the problem (e.g. Li et al. 2015; Lin et al. 2019; Bluck et al. 2020).

ACKNOWLEDGEMENTS

YC is funded by the China Postdoctoral Science Foundation (grant No. 2022TQ0329). HJM thanks T.D. Lee Institute and Shanghai Jiaotong University for hosting his sabbatical during which the work was done. This work is also supported by the National Natural Science Foundation of China (NSFC, Nos. 12192224, 11733004 and 11890693) and CAS Project for Young Scientists in Basic Research (grant No. YSBR-062). YC thanks Kai Wang, Yu Rong, Wentao Luo, Enci Wang, Hao Li and Hui Hong for their valuable insights and discussions. The authors would like to express their gratitude to the Tsinghua Astrophysics High-Performance Computing platform at Tsinghua University and the Supercomputer Center of the University of Science and Technology of China for providing the necessary computational and data storage resources that have significantly contributed to the research results presented in this paper. The computations and presentations in this paper are supported by various software tools, including the HPC toolkits HIPP (Chen & Wang 2023)¹ and PyHIPP², interactive computation environment IPYTHON (Perez & Granger 2007), numerical libraries NUMPY (Harris et al. 2020), ASTROPY (Robitaille et al. 2013; Astropy Collaboration et al. 2018, 2022) and SCIPY (Virtanen et al. 2020), as well as the graphical

library MATPLOTLIB (Hunter 2007). This research has made extensive use of the arXiv and NASA's Astrophysics Data System. Data compilations used in this paper have been made much more accurate and efficient by the software WEBPLOTDIGITIZER.

DATA AVAILABILITY

The code repository TwoPhaseGalaxyModel³ implements the model described Paper-I. All data used in this paper, including data points displayed in figures and observational results used for calibration and comparison, will be distributed along with the repository.

REFERENCES

- Astropy Collaboration et al., 2018, *The Astronomical Journal*, 156, 123
 Astropy Collaboration et al., 2022, *The Astrophysical Journal*, 935, 167
 Behroozi P. S., Wechsler R. H., Conroy C., 2013, *ApJ*, 770, 57
 Bernardi M., Meert A., Vikram V., Huertas-Company M., Mei S., Shankar S., Sheth R. K., 2012, Systematic Effects on the Size-Luminosity Relation: Dependence on Model Fitting and Morphology, [doi:10.48550/arXiv.1211.6122](https://arxiv.org/abs/10.48550/arXiv.1211.6122)
 Bett P., Eke V., Frenk C. S., Jenkins A., Helly J., Navarro J., 2007, *Monthly Notices of the Royal Astronomical Society*, 376, 215
 Bezanson R., van Dokkum P. G., Tal T., Marchesini D., Kriek M., Franx M., Coppi P., 2009, *The Astrophysical Journal*, 697, 1290
 Blank M., Macciò A. V., Dutton A. A., Obreja A., 2019, *Monthly Notices of the Royal Astronomical Society*, 487, 5476
 Bluck A. F. L., Maiolino R., Sánchez S. F., Ellison S. L., Thorp M. D., Piotrowska J. M., Teimoorinia H., Bundy K. A., 2020, *Monthly Notices of the Royal Astronomical Society*, 492, 96
 Bullock J. S., Dekel A., Kolatt T. S., Kravtsov A. V., Klypin A. A., Porciani C., Primack J. R., 2001, *ApJ*, 555, 240
 Burkert A., et al., 2016, *ApJ*, 826, 214
 Chen Y., Wang K., 2023, Astrophysics Source Code Library, p. ascl:2301.030
 Ciotti L., Lanzoni B., Volonteri M., 2007, *The Astrophysical Journal*, 658, 65
 Conroy C., 2013, *Annual Review of Astronomy and Astrophysics*, 51, 393
 Cui W., Davé R., Peacock J. A., Anglés-Alcázar D., Yang X., 2021, The Origin of Galaxy Colour Bimodality in the Scatter of the Stellar-to-Halo Mass Relation (arxiv:2105.12145), [doi:10.48550/arXiv.2105.12145](https://arxiv.org/abs/10.48550/arXiv.2105.12145)
 Davé R., Anglés-Alcázar D., Narayanan D., Li Q., Rafieferantsoa M. H., Appleby S., 2019, *Monthly Notices of the Royal Astronomical Society*, 486, 2827
 Deng Y., Li H., Kannan R., Smith A., Vogelsberger M., Bryan G. L., 2024, *Monthly Notices of the Royal Astronomical Society*, 527, 478
 Desmond H., Wechsler R. H., 2015, *Monthly Notices of the Royal Astronomical Society*, 454, 322
 Fan L., Lapi A., De Zotti G., Danese L., 2008, *The Astrophysical Journal*, 689, L101
 Graham A. W., 2013, in Oswalt T. D., Keel W. C., eds., Planets, Stars and Stellar Systems: Volume 6: Extragalactic Astronomy and Cosmology. Springer Netherlands, Dordrecht, pp 91–139, [doi:10.1007/978-94-007-5609-0_2](https://arxiv.org/abs/10.1007/978-94-007-5609-0_2)
 Graham A. W., Sahu N., 2023, *Monthly Notices of the Royal Astronomical Society*, 518, 2177
 Greene J. E., Strader J., Ho L. C., 2020, *Annual Review of Astronomy and Astrophysics*, 58, 257
 Guo Y., et al., 2009, *Monthly Notices of the Royal Astronomical Society*, 398, 1129
 Harris C. R., et al., 2020, *Nature*, 585, 357
 Hearin A. P., Chaves-Montero J., Becker M. R., Alarcon A., 2021, *The Open Journal of Astrophysics*, 4, 7

¹ <https://github.com/ChenYangyao/hipp>

² <https://github.com/ChenYangyao/pyhipp>

³ <https://github.com/ChenYangyao/two-phase-galaxy-model>

Hopkins P. F., Bundy K., Hernquist L., Wuyts S., Cox T. J., 2010a, *Monthly Notices of the Royal Astronomical Society*, 401, 1099

Hopkins P. F., et al., 2010b, *The Astrophysical Journal*, 715, 202

Hopkins P. F., et al., 2018, *Monthly Notices of the Royal Astronomical Society*, 480, 800

Hopkins P. F., et al., 2023a, *Monthly Notices of the Royal Astronomical Society*, 519, 3154

Hopkins P. F., et al., 2023b, *Monthly Notices of the Royal Astronomical Society*, 525, 2241

Huang K.-H., et al., 2017, *The Astrophysical Journal*, 838, 6

Hunter J. D., 2007, *Computing in Science & Engineering*, 9, 90

Ito K., et al., 2023, Size - Stellar Mass Relation and Morphology of Quiescent Galaxies at $z \geq 3$ in Public JWST Fields, doi:10.48550/arXiv.2307.06994

Ji Z., Giavalisco M., 2022, *ApJ*, 935, 120

Ji Z., Giavalisco M., 2023, *ApJ*, 943, 54

Kormendy J., Kennicutt Jr. R. C., 2004, *Annual Review of Astronomy and Astrophysics*, 42, 603

Kravtsov A. V., 2013, *The Astrophysical Journal*, 764, L31

Lange R., et al., 2015, *Monthly Notices of the Royal Astronomical Society*, 447, 2603

Li C., et al., 2015, *The Astrophysical Journal*, 804, 125

Li H., Vogelsberger M., Marinacci F., Sales L. V., Torrey P., 2020, *Monthly Notices of the Royal Astronomical Society*, 499, 5862

Lin L., et al., 2019, *The Astrophysical Journal*, 872, 50

Lotz J. M., Jonsson P., Cox T. J., Croton D., Primack J. R., Somerville R. S., Stewart K., 2011, *The Astrophysical Journal*, 742, 103

Lu Y., Mo H. J., Katz N., Weinberg M. D., 2006, *Monthly Notices of the Royal Astronomical Society*, 368, 1931

Ma X., et al., 2020, *Monthly Notices of the Royal Astronomical Society*, 493, 4315

Macciò A. V., Dutton A. A., Van Den Bosch F. C., Moore B., Potter D., Stadel J., 2007, *Monthly Notices of the Royal Astronomical Society*, 378, 55

McCluskey F., Wetzel A., Loebman S. R., Moreno J., Faucher-Giguère C.-A., 2023, Disk Settling and Dynamical Heating: Histories of Milky Way-mass Stellar Disks across Cosmic Time in the FIRE Simulations, doi:10.48550/arXiv.2303.14210

Miller T. B., van Dokkum P., Mowla L., van der Wel A., 2019, *ApJL*, 872, L14

Mishra P. K., Rana D., More S., 2023, *Monthly Notices of the Royal Astronomical Society*, 526, 2403

Mo H. J., Mao S., White S. D. M., 1998, *Monthly Notices of the Royal Astronomical Society*, 295, 319

Mo H., Chen Y., Wang H., 2023, A Two-Phase Model of Galaxy Formation: I. The Growth of Galaxies and Supermassive Black Holes (arxiv:2311.05030), doi:10.48550/arXiv.2311.05030

Mowla L., van der Wel A., van Dokkum P., Miller T. B., 2019, *ApJL*, 872, L13

Murray S., 2014, *Astrophysics Source Code Library*, p. ascl:1412.006

Naab T., Johansson P. H., Ostriker J. P., 2009, *The Astrophysical Journal*, 699, L178

Navarro J. F., Frenk C. S., White S. D. M., 1997, *ApJ*, 490, 493

Nedkova K. V., et al., 2021, *Monthly Notices of the Royal Astronomical Society*, 506, 928

Newman A. B., Ellis R. S., Bundy K., Treu T., 2012, *The Astrophysical Journal*, 746, 162

Oser L., Ostriker J. P., Naab T., Johansson P. H., Burkert A., 2010, *The Astrophysical Journal*, 725, 2312

Oser L., Naab T., Ostriker J. P., Johansson P. H., 2012, *The Astrophysical Journal*, 744, 63

Perez F., Granger B. E., 2007, *Computing in Science and Engineering*, 9, 21

Planck Collaboration et al., 2016, *Astronomy and Astrophysics*, 594, A13

Robitaille T. P., et al., 2013, *A&A*, 558, A33

Saha, K. Martínez-Valpuesta, I. Gerhard, O. 2012, *EPJ Web of Conferences*, 19, 06008

Saha K., Tseng Y.-H., Taam R. E., 2010, *The Astrophysical Journal*, 721, 1878

Schaye J., et al., 2015, *Monthly Notices of the Royal Astronomical Society*, 446, 521

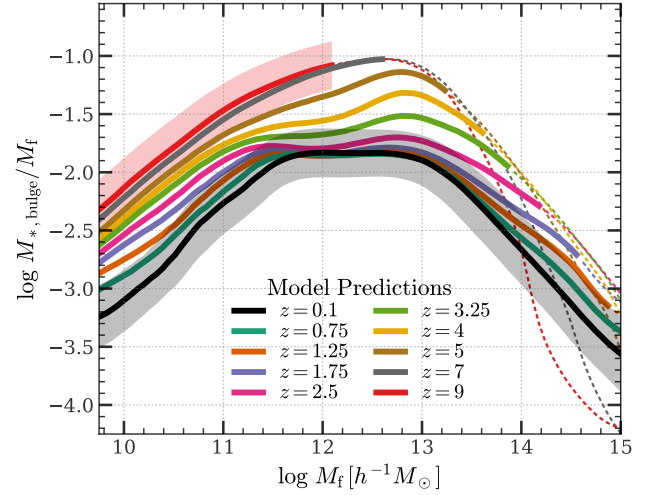


Figure A1. The ratio of bulge stellar mass ($M_{*,\text{bulge}}$) to halo mass assembled in the fast phase (M_f) as a function of M_f , predicted by our model at different redshifts. Here, dynamically hot galaxies, defined as those with a bulge stellar mass fraction $f_{\text{bulge}} > 0.75$ (see §3.1), are included in the analysis. The curves represent median relations, while shaded areas indicate the 16th–84th percentile ranges (shown only for the two extreme redshifts for clarity). The dashed tail of each curve marks the range of halo mass where the halo mass function is lower than $1.0 h^3 \text{Gpc}^{-3} \text{dex}^{-1}$ and thus the hosted galaxies are too rare to be observed. The plateau feature of these curves is inferred as the reason for the $r_{\text{bulge}}-M_{*,\text{bulge}}$ relation to follow the r_f-M_f relation at $M_f \approx 10^{12} M_{\odot}$ (see §3.2).

Shen S., Mo H. J., White S. D. M., Blanton M. R., Kauffmann G., Voges W., Brinkmann J., Csabai I., 2003, *Monthly Notices of the Royal Astronomical Society*, 343, 978

Shi Y., Kremer K., Grudić M. Y., Gerling-Dunsmore H. J., Hopkins P. F., 2023, *Monthly Notices of the Royal Astronomical Society*, 518, 3606

Somerville R. S., et al., 2008, *The Astrophysical Journal*, 672, 776

Somerville R. S., et al., 2018, *Monthly Notices of the Royal Astronomical Society*, 473, 2714

Suess K. A., Kriek M., Price S. H., Barro G., 2019, *The Astrophysical Journal*, 877, 103

Virtanen P., et al., 2020, *Nat Methods*, 17, 261

Wechsler R. H., Bullock J. S., Primack J. R., Kravtsov A. V., Dekel A., 2002, *ApJ*, 568, 52

Weinberger R., et al., 2017, *Monthly Notices of the Royal Astronomical Society*, 465, 3291

Weinberger R., et al., 2018, *Monthly Notices of the Royal Astronomical Society*, 479, 4056

Yang X., Mo H. J., van den Bosch F. C., 2003, *Monthly Notices of the Royal Astronomical Society*, 339, 1057

Yang X., Mo H. J., van den Bosch F. C., Zhang Y., Han J., 2012, *ApJ*, 752, 41

Zhao D. H., Mo H. J., Jing Y. P., Börner G., 2003, *Monthly Notices of the Royal Astronomical Society*, 339, 12

Zhuang M.-Y., Ho L. C., 2023, *Nat Astron*, pp 1–14

van Dokkum P. G., et al., 2008, *The Astrophysical Journal*, 677, L5

van Dokkum P. G., et al., 2015, *The Astrophysical Journal*, 813, 23

van der Wel A., et al., 2014, *The Astrophysical Journal*, 788, 28

van der Wel A., et al., 2024, *The Astrophysical Journal*, 960, 53

APPENDIX A: STAR FORMATION EFFICIENCY

In §3.2, we have interpreted the non-linear size-mass ($r_{\text{bulge}}-M_{*,\text{bulge}}$) relation of dynamically hot galaxies as a combined con-

sequence of the near-linear halo size-halo mass (r_f - M_f) relation, the homologous bulge size-halo size relation ($r_{\text{bulge}} \approx 100 r_f$), and the non-linear bulge mass-halo mass ($M_{*,\text{bulge}}$ - M_f) relation. Specifically, the follow-up of the r_{bulge} - $M_{*,\text{bulge}}$ relation to the r_f - M_f relation appears at the halo mass where the star formation efficiency ($M_{*,\text{bulge}}/M_f$) reaches its peak, and the non-linear flattening and up-turn of the r_{bulge} - $M_{*,\text{bulge}}$ relation are produced by the suppression of star formation efficiency at lower and higher masses, respectively. Fig. A1 shows the star formation efficiency as a function of M_f predicted by our model at various redshifts. A plateau is seen at $M_f \approx 10^{12} M_\odot$ at $z \approx 0.1$, and it becomes slightly tilted at $z \approx 3$. This feature is expected and thus supports our interpretation of the non-linear size-mass relation of dynamically hot galaxies.

This paper has been typeset from a \LaTeX file prepared by the author.